REPORT DOCUMENTATION PAGE

AFRL-SR-AR-TR-04-

8121

1. REPORT DATE *(DD-MM-YYYY)*	2. REPORT TYPE	3. DATES COVERED *(From - To)*
	Final Report	Jun 1, 02 - May 31, 03

4. TITLE AND SUBTITLE
The design and construction of the Second-Generation Optimized Fabry-Perot doppler Imager (SOFDI)

5a. CONTRACT NUMBER

5b. GRANT NUMBER
F49620-02-1-0259

5c. PROGRAM ELEMENT NUMBER

6. AUTHOR(S)
Dr. J. W. Meriwether

5d. PROJECT NUMBER

5e. TASK NUMBER

5f. WORK UNIT NUMBER

7. PERFORMING ORGANIZATION NAME(S) AND ADDRESS(ES)
Clemson University
Clemson, SC 29634

8. PERFORMING ORGANIZATION REPORT NUMBER

9. SPONSORING/MONITORING AGENCY NAME(S) AND ADDRESS(ES)
Department of the Air Force   4015 Wilson Blvd.
Air Force Office of Scientific Research   Arlington, VA 22203-1954

20040303 206

12. DISTRIBUTION/AVAILABILITY STATEMENT

Distribution Statement A: Approved for public release. Distribution unlimited

13. SUPPLEMENTARY NOTES
DODAAD CODE: 1D5U5
AFOSR Program Manager: Major Paul Bellaire

14. ABSTRACT
 The funding provided by the Air Force DURIP award that was provided in March of 2002 has been used to build a portable multi-purpose state-of the-art triple etalon Doppler imaging FabryPerot interferometer, which has the name of SOFDI. The application of this instrument is primarily to measure automatically winds and temperatures in the upper atmosphere for the mesosphere and thermosphere regions for both nighttime and daytime periods. In these two atmospheric regions the airglow emissions provided by O1 atoms at 630 nm, 011 ions at '732 nm, and OH molecules (molecular bands) make possible the monitoring of temperature and winds during the night simtiltaneously with an accuracy of the order of 5 ms1 in five minutes. Daytime measurements of thermospheric winds using the 630 nm emission of 01 at a slower rate of observation and with somewhat less accuracy is the main goal of the application of this instrument. Because of the demanding nature of this application, a number of significant innovations was introduced in the design of SOFDI. These include simultaneous measurements of four fields of view that are obtained by four separate articulated telescopes, the use of the QuadCLIO and the QuadCLIO cxtender(CLIO means circle to line interferometer optic) to image each high resolution spectrum onto a quadrant of the CCD camera detector.

15. SUBJECT TERMS

16. SECURITY CLASSIFICATION OF:			17. LIMITATION OF ABSTRACT	18. NUMBER OF PAGES	19a. NAME OF RESPONSIBLE PERSON
a. REPORT	b. ABSTRACT	c. THIS PAGE			Dr. J. W. Meriwether
					19b. TELEPHONE NUMBER *(Include area code)*

Final Report: The design and construction of the Second-Generation Optimized Fabry-Perot Doppler Imager (SOFDI)

submitted to the Air Force Office of Scientific Research
(proposal control number 01NM314
AFOSR award number F49620-02-1-0259.)

Principal Investigator:
J. W. Meriwether
Clemson University
Clemson, SC 29634
Tel. 864-656-4349
E-mail: john.meriwether@ces.clemson.edu

February 16, 2004

Summary

The funding provided by the Air Force DURIP award that was provided in March of 2002 has been used to build a portable multi-purpose state-of-the-art triple etalon Doppler imaging Fabry-Perot interferometer, which has the name of SOFDI. The application of this instrument is primarily to measure automatically winds and temperatures in the upper atmosphere for the mesosphere and thermosphere regions for both nighttime and daytime periods. In these two atmospheric regions the airglow emissions provided by OI atoms at 630 nm, OII ions at 732 nm, and OH molecules (molecular bands) make possible the monitoring of temperature and winds during the night simultaneously with an accuracy of the order of 5 ms^{-1} in five minutes. Daytime measurements of thermospheric winds using the 630 nm emission of OI at a slower rate of observation and with somewhat less accuracy is the main goal of the application of this instrument. Because of the demanding nature of this application, a number of significant innovations was introduced in the design of SOFDI. These include simultaneous measurements of four fields of view that are obtained by four separate articulated telescopes, the use of the QuadCLIO and the QuadCLIO extender (CLIO means circle to line interferometer optic) to image each high resolution spectrum onto a quadrant of the CCD camera detector, the use of fiber optics to pass the signals from the telescopes to the SOFDI optics, a unique means of obtaining an absolute calibration of Doppler shift with reference to the laboratory emission wavelength of the 630 nm emission, and the ability to select remotely any one combination of the three etalons for a particular science application. This report provides the details regarding the design and construction of this instrument incorporating these unique refinements provided by modern optical technology.

Contents

1 Introduction

An important area of space weather studies is thermospheric dynamics. Variations of the ion-neutral collisional coupling will occur in the F-region depending on the direction and magnitude of the thermospheric winds. These effects need to be characterized because this "ion drag" coupling will modify the F-layer ionospheric structure by changing its vertical profile and its height. Ground-based studies of thermospheric dynamics with optical instrumentation have been previously limited to nighttime measurements because the range of sky continuum brightness between night and day is enormous, $\sim 10^{12}$, making the task of observing the 630 nm dayglow extremely challenging. This emission of atomic oxygen exists in a region between 150 and 250 km with most of the emission occurring above 175 km where the high viscosity of the thermosphere region removes any significant vertical variation of wind and temperature over this range of altitudes. This region of airglow emission shifts by about 50 km to higher altitudes at night.

Observing upper atmosphere winds during the day with such high continuum background calls for an optical instrument that truly represents modern technology not normally available to university researchers. Accordingly, our DURIP proposal submitted to the Air Force Office of Scientific Research in August 2001 and funded in March 2002 requested funds to buy a Second-generation Optimized Fabry-Perot Doppler Imager interferometer (SOFDI) instrument from the Michigan Aerospace Corporation (MAC) that would be capable of such measurements.

The SOFDI instrument is a triple etalon Fabry-Perot interferometer designed with the capability of relocatable etalons so that the instrument can be reconfigured to have one, two, or three etalons aligned for specific science studies. These etalons are specified for resolutions ranging from a high resolution (HRE) to medium (MRE) to low (LRE). The three etalons must be well-aligned so that the overlapping transmission functions effectively reduce the overall spectral width from that of the interference filter to that of the HRE passband, typically 0.05 Å. Light is received from four independent articulated telescope systems through fiber optics cables. After passing through the full aperture of the series of aligned etalons (whether one, two, or all three) to the QuadCLIO optic, the high resolution spectrum for each of the four fields of view is sent through the QuadCLIO extender and imaged upon a separate quadrant of the CCD camera. The collected spectra for the four CCD quadrants are then analyzed to retrieve temperatures, line-of-sight Doppler shifts, and airglow intensity and sky background for each of the four separate directions. This capability allows the thermospheric winds and temperatures to be measured in four separate direction simultaneously for either nighttime or daytime periods. In the case of daytime measurements it is intended that one of the four directions would be dedicated to the continual observation of the solar continuum that can be removed for the spectrum obtained for each of the other three directions.

The design of the SOFDI instrument is based upon that of the High Resolution Doppler Imager that was flown on the NASA Upper Atmosphere Research Satellite but modernized in a variety of ways to improve its already robust design. This instrument would be applied to study daytime thermospheric dynamics with particular reference to the ion-neutral coupling that is characteristic of the equatorial thermosphere or the polar region. Because this coupling is key to the potential forecasting of scintillation activity that impacts communication channel quality, this issue is a topic of great interest to the Air Force.

The instrument is designed to operate automatically via the Internet. It is housed within a thermally-controlled pressure chamber inside a

portable research trailer.

SOFDI daytime capability would be especially valuable for the ground-based support of C/NOFS, an Air Force satellite charged with the mission to characterize the environment that is conducive to scintillation activity and plasma structuring. This satellite is now scheduled to fly in the fall of 2004. SOFDI daytime measurements obtained at the magnetic equator location of Huancayo, Peru, would provide valuable confirmation of the in situ measurements of equatorial winds obtained by the C/NOFS sensor, which does not have any separate means of validation.

As a bonus, the SOFDI FPI instrument is designed to be switched to a nighttime mode to observe nighttime thermospheric dynamics with excellent accuracy. This high sensitivity combined with excellent instrumental stability will make possible the routine measurements of vertical winds of 1 to 5 m/s with good accuracy. This vertical wind capability would open new directions of research in thermospheric dynamics for both equatorial and polar regions.

Application of this instrument in any measurement program would require operating funds to cover the expected expenses and additional support from a post-doctoral associate and MAC. Consequently, a NSF proposal for such funds was submitted to the Coupling Energetics Dynamics of Atmospheric Regions (CEDAR) program in May 2002 that was successful. A search for a post-doctoral associate commenced and culminated in the hiring of Prof. Andrew Gerrard who was trained as a lidar scientist at the Pennsylvania State University and was an assistant professor at the State University of New York at the Morrisville campus in upstate New York. He was particularly well suited for the position because he had developed an expertise in the area of signal processing as part of his engineering background and also displayed a strong interest in applications of remote sensing. Such experience was helpful in developing a forward model for the analysis of the daytime spectra that we would be acquiring with SOFDI.

Because it is expected that a great deal of software development and hardware trial operations will be necessary, we also proposed to NSF the idea of collaborative research with Millstone Hill Observatory. This was funded with a SGER (Special Grant for Enterprising Research) award. Such awards are designed to support innovative research. In our case, the plan was to relocate the SOFDI observatory from Ann Arbor to upstate New York, to Dr. Gerrard's residence which inspection showed to be an excellent site for airglow measurements. Also important was that this site was ideal for the bistatic observations of thermospheric winds with the Millstone Hill incoherent scatter radar and optical observatories located at Westford, MA. This plan would provide the capability of obtaining overlapping FPI and radar measurements of thermospheric winds and temperatures in the daytime.

The application of SOFDI does not need to be limited to the thermospheric emission of the 630 nm emission but can be extended to other airglow emissions as well. We have incorporated in the design of SOFDI a filter wheel that can be applied to select one of six different filters. Table 1 lists the filter wavelengths and indicates the chief science application pertaining to each choice of filter.

This report presents a summary of the design and fabrication of the SOFDI instrument. Many of SOFDI features represent unique aspects of Fabry-Perot interferometer (FPI) design never before tried in ground-based FPI observatories. An instrument of this complexity is expected to take 12 to 18 months for completion. Unfortunate delays in the delivery of several critical components (etalons, lenses, CCD camera) have meant that the initial phase of the SOFDI integration was not reached until the late fall of 2003, 14 months after the initiation of the design process. At the present time of mid-February 2004, the instrumental assembly

4

Wavelength	Emitter	Science Application
557.7 nm	OI	nighttime mesospheric winds and temperatures
630.0 nm	OI	nighttime and daytime measurements of thermospheric winds and temperatures
632.8 nm		HeNe frequency stabilized laser reference
732.0 nm	O^+	thermospheric ion drifts and temperatures during twilight and possibly daytime
840.0 nm	OH	mesospheric winds and temperature, nighttime
846.6 nm	OH	mesospheric temperatures during daytime from analysis of intensity ratios with 840 nm emissions

Table 1: List of filter wavelengths for SOFDI science applications.

has been completed and the testing of the operations of SOFDI has been underway. Bad weather has thus far prevented any acquisition of nighttime or daytime spectra. Initial tests have confirmed that signals levels will be in accord with expectations. The potential for interesting and exciting science is enormous, and most likely, we will be occupied for many years in realizing the science that is represented by the SOFDI instrument.

2 Theory of the Fabry-Perot interferometer

The Fabry-Perot interferometer is a well-known instrument that has been applied over four decades to the measurements of nighttime thermospheric winds and temperatures. However, application to the daytime calls for a much more sophisticated form of the Fabry-Perot than is normally used for nighttime measurements. The principles of the FPI instrument have been thoroughly reviewed elsewhere and the details will not be repeated here. A good reference is that of Born and Wolfe (Principles of Optics, Cambridge University Press, 1999) and another source regarding the Fabry-Perot is the monograph on the Fabry-Perot Interferometer written by G. Hernandez (Cambridge University Press, 1987).

The etalon of a FPI consists of two flat transparent plates of glass that are mounted to be parallel with a separation gap,d, and with internal faces coated with a mirror surface with reflectivity, R. Peak transmission occurs over a series of n orders when

$$n\lambda = 2\mu d\cos\theta$$

where θ is the angle through the FPI etalon relative to the normal to the etalon plate, μ is the refractive index of the medium between the plates (and is sensitive to density variations), and λ is the wavelength of the light ray at angle θ. The lack of any angular dependence about the optical axis in this expression indi-

cates azimuthal symmetry for the interferogram and indeed, what is observed is a series of circular interference orders appearing as equal-area rings concentric with the optical axis. The pixel spacing between orders decreases in proportion to the square root of the radius from the optical axis. The higher frequency orders lie closer to the optical axis, i.e., the wavelength scale varies from blue to red as the angle θ increases. The spectral distance between orders is designated as the free spectral range, and for SOFDI, the free spectral ranges for the HRE, MRE, and LRE etalons are 0.198 Å, 1.064 Å, and 8.25 Å, respectively.

The essence of the SOFDI instrument approach to daytime measurements is based upon the reduction of the overall instrumental spectral width through the combination of etalon transmission functions at three different resolutions. This approach achieves high spectral resolution, ~ 0.050Å, and converts the interferometer into a monochromator with a resolution represented by the spectral width of the HRE order. The elimination of the FPI sidebands is essential to the successful extraction of the source daytime 630 nm emission profile against the continuum background containing the Fraunhofer spectral structure.

The number of photons, $N(\lambda)$, at a particular wavelength,λ, detected on the CCD from a volume filled emission source, $S(\lambda)$, may be represented as

$$
N(\lambda) = \left[S(\lambda)d\lambda \cdot F(\lambda) \right]
$$
$$
\cdot \left[A_{tele} \cdot \Omega \right] \cdot \left[t \cdot T_{sys} \right]
$$
$$
* \left[\left[T_{HRE}(\lambda) \cdot T_{MRE}(\lambda) \cdot T_{LRE}(\lambda) \cdot IIT(\lambda) \right] \right.
$$
$$
\left. * [D(\lambda)] \right]
$$

where $*$ denotes the convolution operator, and $F(\lambda)$ is the passband of the interference filter, A_{tele} is the area of a telescope, Ω is the receiver field of view expressed as a solid angle, t is the integration time, T_{sys} is the transmission of the the entire receiver chain (including the quantum efficiency of the CCD and the coupling efficiency and transmission through the fiber optic cables) excluding the etalons, $T_{HRE}(\lambda), T_{MRE}(\lambda), T_{LRE}(\lambda)$ are the transmission functions for the high resolution, medium resolution, and low resolution etalons, respectively, $IIT(\lambda)$ is the multiplicative term representing the incoherent intercavity transmission of the etalon system (as discussed in Skinner, Hays, and Abreu [Appl. Optics, 26, 2817-2827, 1987] and expressed as their equation 10), and $D(\lambda)$ is the defect function of the etalon plates. The first term on the right-hand-side of this equation represents the spectral distribution of photons "availible" to the receiver and the second term is the well-known etendue of the system. The product of the first three terms is convolved with the remaining term, which represents the spectral transmission of the three etalons.

The source function represents the spectral distribution with wavelength of OI (^{1}D) photons emitted by thermospheric atomic oxygen atoms. This distribution is assumed to be well-represented by a Maxwellian distribution characterized by the Doppler central position, the Doppler broadening, the spectral intensity, and the continuum background. The etalon functions may be approximated by Airy functions as specified by the choice of the spacer gap for each etalon. The reflectivity chosen for SOFDI etalon surfaces was $\sim 87\%$ so the finesse for each etalon is typically 15.

The spacer gaps are chosen so that the overlapping transmissions of the three etalon passbands in series with a narrow interference filter would reduce the instrumental spectral width from ~ 5 Å to ~ 0.05 Å and thereby reduce the continuum background by two orders of magnitude. The Doppler shift of the dayglow emission of OI at 630 nm and the Doppler broadening of the spectral emission profile would yield

6

the thermospheric line-of-sight speed and temperature as averaged over the dayglow volume emission profile between 175 and 275 km.

A complication is the fact that the 630 nm airglow emission line is located within a Fraunhofer valley approximately 5% deep that shifts in wavelength by as much as 600 m^{-1} depending on the direction of the Sun as a function of local time. This shift is a result of the introduction of a Doppler shift by the rotational speed of the Earth relative to the spectral position of the solar Fraunhofer structure. The successful removal of this background requires that the continuum be measured separately simultaneously with the acquisition of the 630 nm dayglow spectrum. Previous work in the application of the triple etalon FPI had had difficulty with this problem in that the measurements were obtained either separately or interleaved with the sky measurements thus introducing the possibility of small errors that might be serious when accumulated over a significant interval of time. The specifications for the three etalons of the SOFDI instrument are given in Table 2.

3   Trailer housing

An issue that had to be addressed immediately prior to the start of the design phase of SOFDI was how to achieve the desired portability of this instrument. Considerable thought convinced us that a trailer that could be attached to a truck or a 4WD vehicle was the best solution with respect to the engineering issues of thermal environmental control and ease of shipping. The enclosure must be big enough to house all of the necessary power, air and thermal conditioning, as well as space for the two instruments of SOFDI and an all-sky imager. The all-sky imager would provide complementary coverage of the mesospheric airglow dynamics. However, there was also the constraint that the trailer must be small enough to fit into a

standard shipping container that is 20 feet long.

The expense of the construction of the trailer for the SOFDI Observatory was not included within the DURIP budget as it was expected that the necessary funding could be secured from the National Science Foundation and other sources. This did prove to be the case. The Aeronomy Program at NSF provided a SGER award to enable the operations of SOFDI as part of a New England collaborative research project that would have SOFDI conduct an extended campaign of observations in the location of upstate New York, near the city of Oneida at the residence of Dr. Andrew Gerrard. This award covered half of the expense for the trailer, the Clemson Physics Department contributed $10,000 toward the construction expense of this trailer, and the remainder was covered by the Huancayo NSF award provided by the CEDAR program to support the application of SOFDI to daytime thermospheric wind measurements at the magnetic equator. This award is intended to cover the expense of shipping SOFDI to the equatorial location of Huancayo, Peru, in 2004 and, in collaboration with the Instituto del Geofisica Peru (IGP), to undertake a period of extended operations in support of C/NOFS and the operations of the Jicamarca Radar Observatory.

Figure 1 presents a view of the SOFDI Observatory that was constructed. A Wells-Fargo trailer was purchased and extensively remodeled with insulation added and the trailer equipped with heaters and air conditioning to maintain a thermal range of 70±2°F. A Programmable Logic Control bus was added to achieve the remote switching of the AC power feasible via the Internet. The AC main power input may be of several different forms: 220 three phase or 240 single phase. The total SOFDI Observatory weight was estimated to be 1500 kgs, and the maximum electric power consumption was estimated to be 10 kwatts. At a particular observatory location jacks would be released to take the trailer weight off the tires

7

Parameter	HRE	MRE	LRE
Gap	1.0007 cm	0.186 cm	0.024 cm
Coated diameter	8.8 cm	8.8 cm	8.8 cm
Reflectivity	0.86	0.86	0.86
Coating materials	ZnS-ThF4	ZnS-ThF4	ZnS-ThF4
Etalon material	Fused Silica	Fused Silica	Fused Silica
Type	Fixed spacer	Piezoelectric	Piezoelectric
Num Orders@630 nm	12.5	~2.3	~0.3
Post material	zerodur	PZT-5H	PZT-5H
Field of View	0.028 half angle	0.028 half angle	0.028 half angle

Table 2: Specifications of the SOFDI triple etalons.

and stabilize the trailer against wind motion. An lightning arrestor will provide protection against possible lightning strikes. An alarm system will prevent any unauthorized instrusion into the trailer. A web camera mounted in the forward part of the trailer provides the monitoring of cloud cover that can be passed over the Internet and saved as part of archived data to document the possible existence of clouds.
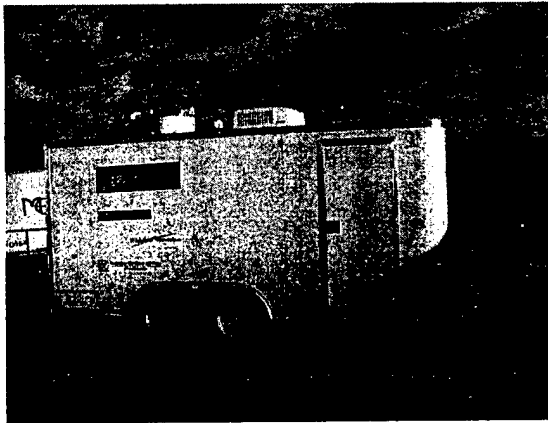

Figure 1: View of the SOFDI Observatory located in the MAC parking lot. The telescopes are visible within the dome enclosures. Not mounted in this view is the all-sky imaging system andits dome which would be located at the left end of the trailer.

4 Instrument overview

Figure 3 presents a schematic showing the overall configuration of the SOFDI instrument. It illustrates the fiber optics cabling, the three etalons that may be translated into or out of the optical path, the CLIO extender, the Quad-CLIO, and the CCD camera. Each of the four fiber optics cables is connected to the output of a telescope system that can be articulated to cover nearly 75% portion of the whole sky. A single face of the QuadCLIO, Circle to Line Interferometer Optic, is a reflective 90° cone that theoretically would transform a 90 degree arc into a point on the optical axis. A QuadCLIO has four such cones transforming each of the four quadrants, each of which represents a separate field of view defined by the telescope system. We will discuss the QuadCLIO and the CLIO extender optics in separate sections below.

Not included in this diagram is the extensive monitoring of the thermal environment of each etalon and of the pressure chamber temperature, room temperature, and the exterior temperature. The reason for such a network of thermistor sensors is that the SOFDI instrumental stability relative to Doppler shifts is directly dependent upon the density and therefore, indirectly, the environmental temperature. By monitoring the temperature closely, it will be possi-

8

ble to generate corrections to the Doppler zero speed position that is crucial to the accurate determination of Doppler shifts. For this reason it is also necessary to house the three etalons within a pressure chamber with walls that are sufficiently stiff to reduce the long-term effects of atmospheric pressure variations. Such pressure variations, if not minimized by the chamber design, would translate into an instrumental shift of the Doppler reference which would impact upon the ability of the instrument to determine line-of-sight winds by detecting Doppler shifts with reference to a zero.

An example of such an instrumental drift is illustrated in Figure 2 which shows the measurements of the position of the several fringes over a period of 3.75 days. In this experiment the pressure chamber was not sealed. The largest change observed, 5 pixels, corresponds to an approximate drift of 500 ms^{-1}, which is unacceptable. This run was repeated with the chamber sealed, and the results show that the instrument was much more stable but there still remains a pressure leak. We expect this behavior would be much improved once the other instrumental problems have been cleared up, and there is time to search for and seal any remaining pressure leaks.

The light from the four line-of-sight fields (each about 2.5 degrees angular width) is transmitted to the filter wheel assembly with fiber optics cables purchased form Fiberoptics Corporation. Each cable contains ~500 fibers. There is a loss of signal caused by the interstices (open space) that exist between these fibers of about 50%. The transmission along each fiber is about 90 %. The loss of light caused by the choice of fiber optics coupling between SOFDI and the telescope systems is compensated by the pointing flexibility provided in which simultaneous collection of signal for each of the four fields independently directed toward the sky can be attained. This capability avoids the loss of time represented by the time it would take to move the telescope
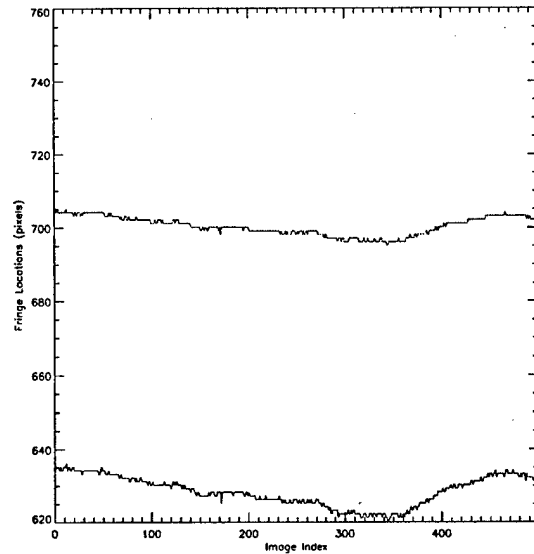

Figure 2: Observed instrumental drift of the SOFDI instrument without pressure control. Plotted are the fringe positions of the three innermost orders of the FPI ring pattern (no CLIO optic installed) relative to the ring center.
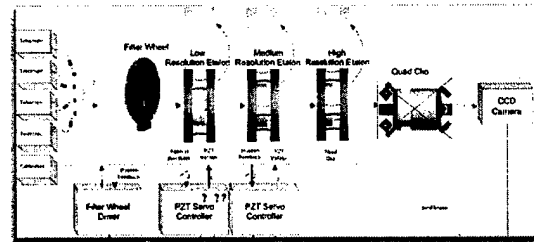

Figure 3: A block diagram illustrating SOFDI components. Fiber optics cable transfer the light from each of the four telescopes to the collimator section of the SOFDI optics. Each of the three etalons can be translated into or out of the optical path.

system from one direction to another. With the SOFDI instrument it would be feasible to consider an observing strategy in which one telescope system is scanning through an auroral arc while the three other telescopes are observing the thermospheric wind vector components in three directions simultaneously.

The three SOFDI etalons are mounted on

9

individual slide platforms that may be translated remotely into or out of the optical axis. Tests have demonstrated that such translation can be done repeatedly without a significant modification of the etalon instrument function and with an accuracy of placement of 0.3 pixel at the axis of the optical axis.

The two piezoelectric etalons were carefully characterized before the integration phase by measuring the relationship between ramp high voltage and the etalon gap. Monitoring the etalon gap separation by capacitative feedback provides long-term stability. This calibration effort provided the necessary voltage ramp constants required for each piezoetalon post so that each piezoelectric etalon may be tuned as desired to any specific gap separation. These post values were embedded into the software so to be transparent to the user.

5 SOFDI optical design - simulations

Since the SOFDI instrument design is based upon that of the High Resolution Doppler Imager (HRDI) that was flown on the Upper Atmosphere Research Satellite, it was not necessary to research extensively the optimal choices for the three spacer specifications for the three HRE, MRE, and LRE etalons. The MRE and LRE etalons would have piezo-electric etalon posts so that a passband of each of the two transmission functions of these etalons can be tuned to coincide with a HRE passband thus producing minimization of the transmission of the HRE orders not selected.

The successful experience of HRDI convinced us that we would be well served to use identical etalon gap specifications as that for HRDI. These choices are listed in Table 2. The design consideration here is that rather than have a second etalon that requires a relatively high finesse, the combination of two etalons as represented by the MRE and the LRE etalons,

each possessing a moderate finesse, would be more stable. An etalon with high finesse (which means a high reflectivity (R) for the mirror surface of each etalon plate) has lower throughput as the transmission is weighted by the factor of $\frac{1-R}{1+R}$. Furthermore, the ability to choose two-etalon combinations such as the HRE and the LRE provides enhanced flexibility for improved experiments, e.g., in twilight or moonlight, where the ratio of signal to noise is benefited by the increased filtering that the addition of the LRE etalon represents. The ability to select any one of the three etalons allows the precise measurements of the transmission function for each etalon, which will prove to be very useful for accurate data analysis and to verify proper alignment of the instrument.

Figure 4 illustrates a simplified simulation of the instrument functions for each of the three SOFDI etalons for two temperatures, 0 K and 1000 K; Figure 5 presents the results of a more sophisticated simulation based upon a forward model, which includes a modeling of the instrumental effects that distorts the Airy transmission function, i.e., spherical curvature of the plates and surface defects of the coating. As these results show, when we used optimal estimates for the combination of the three etalon transmission functions, the bandwidth is reduced to the spectral width of the central transmission peak which is expected to be a factor of 100 higher in transmission than the side bands seen in the figure (note logarithmic scale). However, more realistic estimates produce a ratio of ~15 to 1. This spectral width is ~0.050 Å, which is nearly the same as that of the ~0.035 ÅDoppler broadening for a temperature of 1000 K but the sideband leakage represented by these bands would contribute to the enhancement of the continuum background signal observed by the detector and thus, would lead to a reduction of the ratio of signal to noise.

Another simulation carried out is presented in Figure 6 which shows the determination of the expected interferogram structure for the O$^+$

emission. This is important to the application of SOFDI for twilight and daytime measurements of ion drifts. This emission offers the potential for the observations of ion drifts by measurements of the line-of-sight Doppler shifts of the O^+ from the ground. The Doppler broadening of this feature would be a measure of the neutral temperature because the lifetime of these ions of 5 seconds implies that there is an insufficient number of collisions of the newly-formed oxygen $O^{+2}P$ ions generated by EUV photo-ionization for the inferred Maxwellian distribution to become equivalent to the ion temperature. The wavelengths used for this simulation were provided by Dr. Tom Slanger, SRI International.
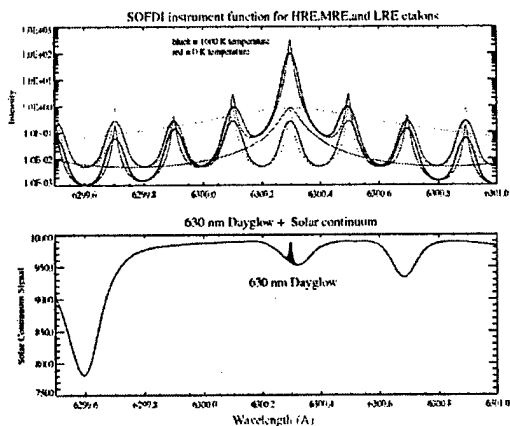
Figure 4: Simulated representation of the SOFDI triple etalon instrument function for two temperatures: 0 K (red) and 1000 K (black). The bottom panel illustrates the solar continuum. The red feature illustrates the dayglow emission of the oxygen OI 630 nm emission at 5% of the dayglow continuum,

6 Telescope systems

Figure 7 illustrates the fiber optics linkage between the SOFDI instrument interior and the four Meade ETX telescope systems. Figure 8 shows two views of the fiber optics cables at
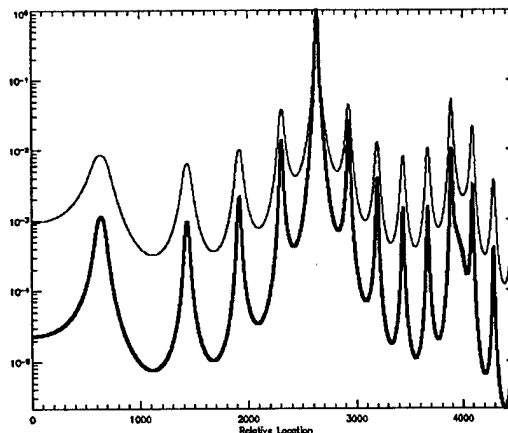

Figure 5: Simulated representation of the SOFDI triple etalon instrument function for 0 K using a forward model. The heavy-line plot illustrates the results for a model that did not include the effects of inter-cavity losses. The light-line plot shows how significant the increase in sideband leakage becomes when a more realistic representation of the effects of inter-cavity losses is included in the model. In the optimal model (no losses) the largest side lobe is decreased relative to the main pass-band by two orders of magnitude whereas a more realistic representation shows that the ratio between these two features is decreased to a value of ~15 to one. The light-line simulation was based upon the work presented by Skinner, Hays, and Abreu in their Applied Optics paper, 1987.

telescope 1 and at the entrance to the SOFDI instrument port. This linkage provides for the illumination of each quadrant of the QuadCLIO optic. The overall transmission was measured to be ~50% for each cable.

Each Meade telescope system is computerized providing the means for a pointing capability to 99% of the sky hemisphere. The telescope aperture is four inches, and the telescope optics were coated with a UV dielectric coating to achieve maximum reflectivity of the telescope mirrors. To avoid the need for physically moving each telescope which would flex the
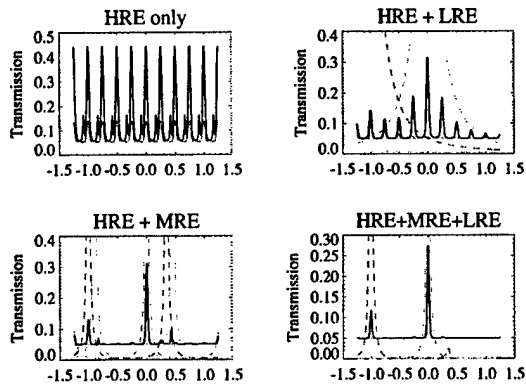
11

Figure 6: Simulated representation of the expected interferogram for different combinations of etalons as indicated in the panel caption. The wavelengths used in this simulation represented by their colors were 7319.044 Å(red), 7320.121Å(green) for the two O^+ components and 7316.282 Å(yellow) for the OH line. These results show that the combination of the HRE and the LRE would provide six orders for the strong O^+ emission without any significant contamination from the OH or the O+ weak emissions.
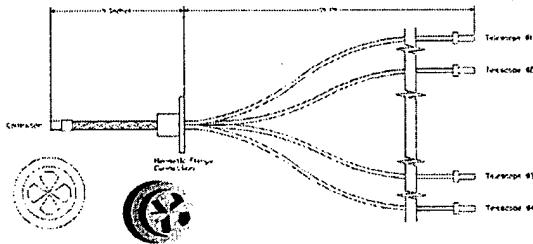
Figure 7: Design layout of fiber optics cabling for transfer of light from telescope to SOFDI collimator.

fiber optics cabling and introduce wear, each telescope system was modified to incorporate a scanning mirror. The mirror over the vertical objective lens section is fixed while the other mirror may be rotated about either horizontal axis of the mirror mount. The conversion of the telescope coordinates into azimuth and zenith angle coordinates is complicated but rep-
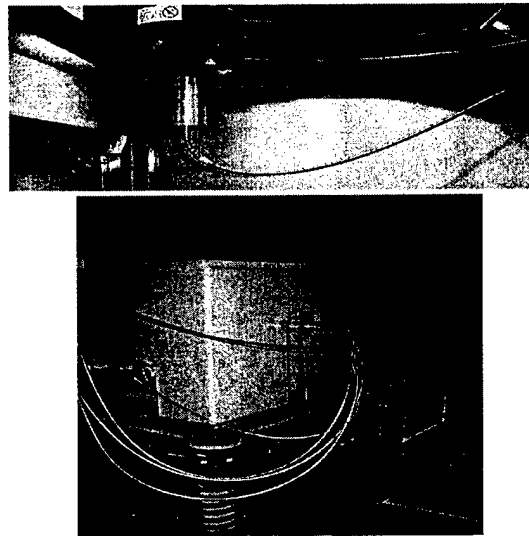

Figure 8: View of the fiber optics cable interface to Telescope 1 (upper panel) and a view of all four cables connected to the SOFDI pressure chamber entrance port (lower panel).

resents a straight-forward geometric transformation. Details are presented in the appendix. The telescope eyepiece is utilized to achieve the correct illumination of the fiber optic cable by adjustment of the focal length.

7 Optical ray-tracing design

The SOFDI optics are relatively complicated and Michigan Aerospace Corporation chose to hire a professional lens designer, Paul Bogert from Luminflow, to undertake the design and specifications of the optics. The results of this study are illustrated in Figure 9. A Zemax ray-tracing program was used to determine the necessary specifications for the optics. The collimator section intentionally introduced a spherical abberation into the input signals so to remove any traces of the fiber optics structure in the source. A holographic diffuser (with 95% transmission) was mounted at the field stop ahead of the collimator section to eliminate the residual effects of this structure (which other-

12

wise was manifested by a "railroad track" signature seen in the QuadCLIO images). Plain glass sheets were inserted between the LRE and MRE etalons and the MRE and the HRE etalons to suppress parasitic ghost interference ring pattern images that would otherwise be introduced by the wedge angle of the etalon front and back surfaces. The light after passing through the etalon section is then passed through a pyramid that is mounted at the entrance to the CLIO extender section. This splits the incoming rays into four separate bundles that are transferred through the CLIO extender into the CLIO with each of the four bundles matching up to a quadrant of the CLIO input. The transformed image from the Quad-CLIO optic is then observed by the CCD camera.

8 CCD camera and etalon fabrication

A study of all the major CCD camera systems that were available for purchase on the market was undertaken to find a camera that would prove to be suitable and inexpensive for SOFDI needs. The requirements for the specifications were low readout noise, a reasonable dark count behavior for an external chiller and a camera thermoelectric cooler, and a relatively fast readout time for the data transfer from the CCD chip to the computer memory. We were satisfied that the dimensions of 1024 x 1024 pixel array with 12 μm square-sized pixels would be suitable for the CLIO image. A study of the possible choices reached the conclusion that the Fingerlake Instrumentation camera would be satisfactory. This company produced an excellent product but the delivery time was much longer than what was stated upon order.

However, this was not the deciding factor in the integration of SOFDI components because we also encountered significant delays in

the delivery of the three etalon plate sets from TecOptics. The specifications for the plate flatness called for $\lambda 150$ flatnesses and a hard coating applied for the reflective surface. The company had to redo the MRE and LRE plates three times before these specifications were satisfied, but very satisfactory results were obtained.
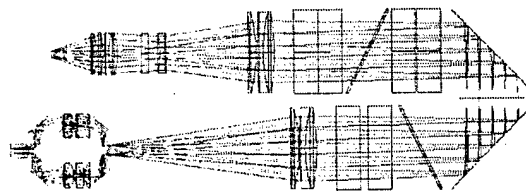

Figure 9: SOFDI optical ray-trace schematics.

The number of orders that would be observed by the SOFDI optics is determined by the overall field of view, the spacer gap, and the wavelength. Figure 10 illustrates the variation of this parameter as a function of wavelength, and one can see that this parameter varies from 14 at 557.7 nm to 8 at 840 nm.
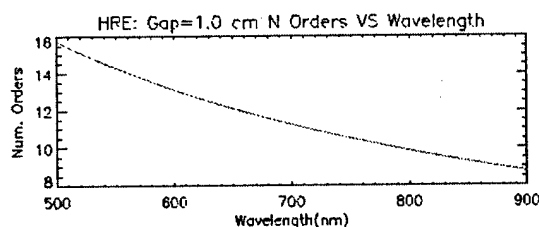

Figure 10: Wavelength variation of the number of orders in CLIO view.

9 QuadCLIO optic and CLIO extender

The QuadCLIO and the CLIO extender illustrated in Figure 12 and Figure 13 are specialized optics that are included in the SOFDI optics chain to perform two functions. The first is to achieve the separability of the fields of view

13

that the application of the QuadCLIO makes possible. (One CLIO transforms a 90° quadrant arc into a point; a QuadCLIO transforms four such quadrants.)

During the design phase it became evident that the four fields of view from the telescopes would overlap physically within the optical path unless the four fields were separated by the CLIO extender. This device transforms the angular dimensions of the four fields so to match up with the required input angles into the CCD camera. A second reason for the inclusion of the CLIO extender is to avoid the need to install the QuadCLIO within the cavity of the CCD camera making the application of the CCD camera simpler without any need for modification of the CCD camera. This enhances the instrumental reliability and simplifies the instrumental integration process.

The second function for the application of the CLIO optic is to minimize the noise addition to the detector signal that would be incurred if the signal pattern seen by the CCD chip during the exposure of the signal to the camera were the circular ring pattern of the HRE. The CLIO optic concentrates the light of each circular quadrant for each order into a linear array of a few pixels before the exposure to the CCD camera takes place. The advantage that this provides is that for weak signals the amplifier noise introduced by the readout of the CCD chip signals would be essentially eliminated as the readout noise is added to the much larger pixel signals that are produced by this concentration of light. and therefore insignificant. This would not be the case without the CLIO optic. Obviously, the CLIO optic would not be of benefit for bright sources such as the aurora or for the daytime application in which the signals are dominated by the large Rayleigh continuum of the daytime sky.

Figure 12, Figure 13, Figure 14 and Figure 15 illustrate further details of the CLIO extender optics in conceptual form and in actual practice as observed in the MAC clean room

Circle-to-Line Interferometer Optical System
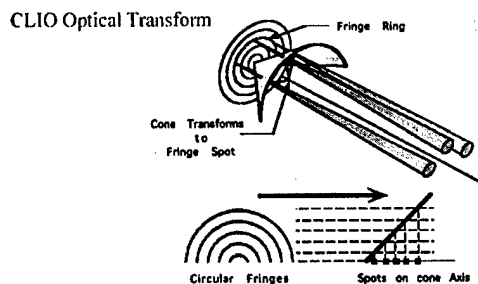US Patent #4,893,003

Figure 11: CLIO conceptual design. An illustration of the transformation of the circular FPI arc into a point on the CCD chip)
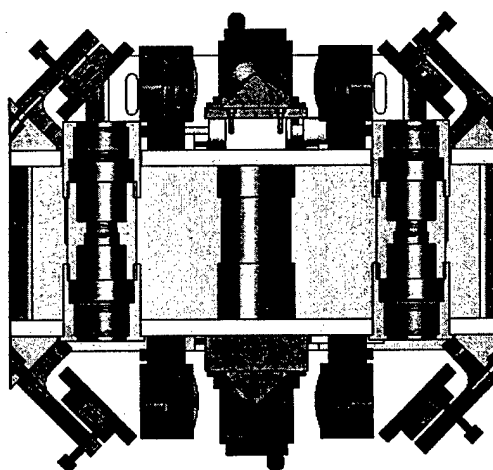

Figure 12: A cutaway view of the CLIO extender. The reflective pyramids may be seen in the bottom and top areas of the figure. The optical axis extends from the top pyramid to the bottom. As light enters the extender assembly at the top, the light for each quadrant is diverted into a separate path where additional optics modify the image size so that the light may be focused upon the front surface of the CCD chip after reflection into the optical path by the bottom pyramid.
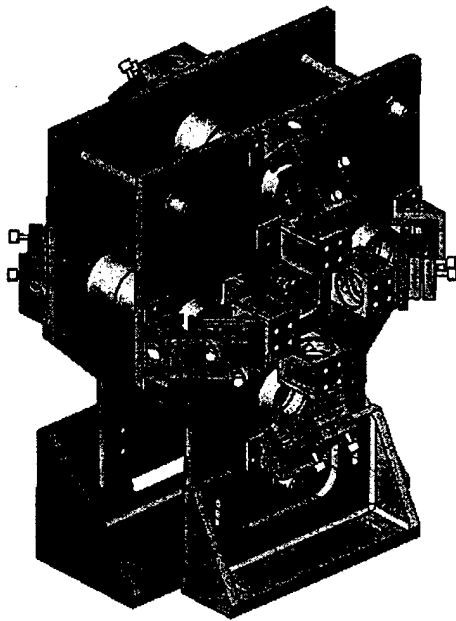
where the extender optics were assembled.

14

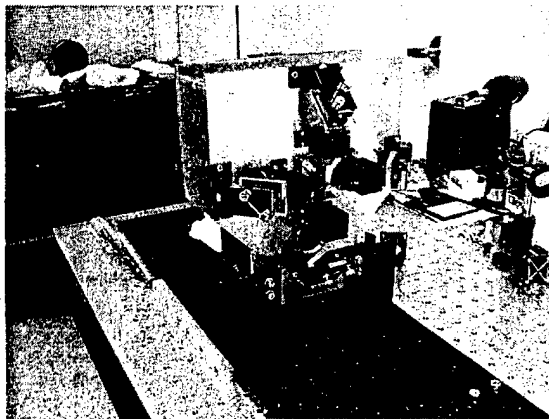Figure 13: An alternative cutaway view of the CLIO extender.

Figure 14: Display of CLIO extender optics in clean room.

10 SOFDI Doppler shift determination

Doppler shift measurements with a FPI are made with respect to a reference that represents a state of zero Doppler shift. SOFDI
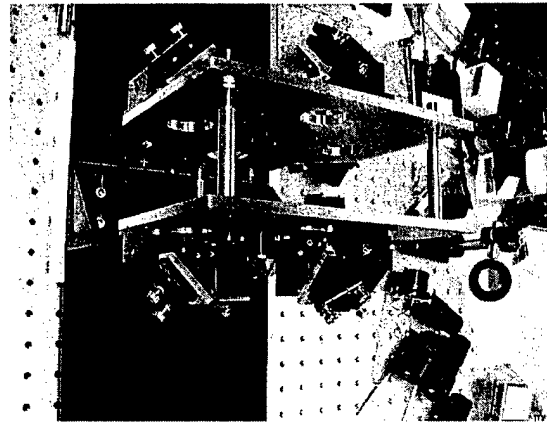

Figure 15: Alternate view of CLIO extender optics in clean room.

will accomplish this through two means: first, by absolute reference to a calibration standard, and secondly, by using measurements from the zenith averaged over a period of time during which the vertical motions of a few ms^{-1} are averaged out. This latter means has been the traditional approach but it is based upon the assumption that vertical winds are generally insignificant when compared with the horizontal winds of 100 to 200 ms^{-1}. SOFDI will supplement this classical means for determining the Doppler reference with the use of measurements from a calibration source that represents a secondary standard. In particular, for the case of 630 nm, the reference emission would be a choice between two sources: cerium, which has a triplet of lines near 630 nm with one line located within the same free spectral range as the 630 nm emission of oxygen, namely, the Ce 6300.212 Å wavelength. The other choice is hafnium which has a single emission line located about 3.8 free spectral ranges away, at 6299.542 Å. We will be making tests to determine which of these is a better choice. Hafnium has more signal but the use of this emission will require that the free spectral range be specified with a precision of 1 ms^{-1}. The cerium emission, although within the same free spectral range as that of the oxygen line, has a com-
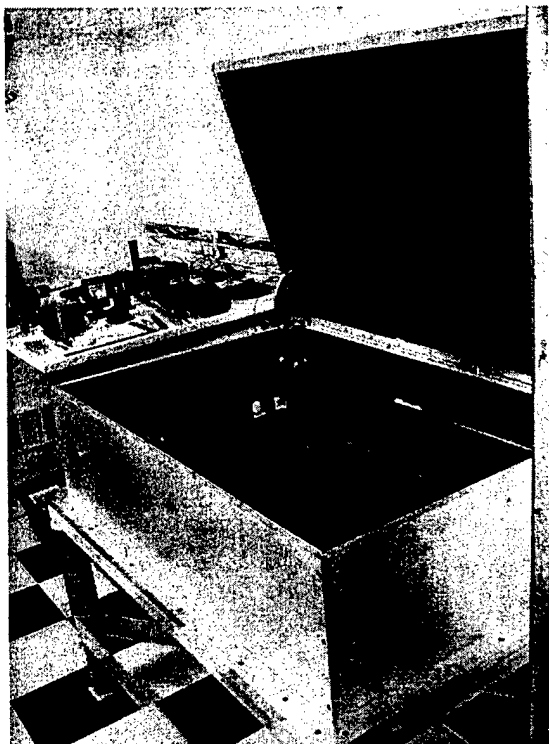
15

Figure 16: SOFDI etalon chamber before installation of optics. Notice the thick walls of aluminum that enhance thermal inertia and minimize effects of atmospheric pressure variations. The base of the chamber is attached to stiff springs that will prevent low frequency vibrations from penetrating into the chamber during transit of the Observatory between observing sites.

plex structure that may hamper the application of this emission to the determination of a zero Doppler reference. The offset between either cerium or hafnium and the oxygen emission will be measured by Prof. Manfred Biondi, at the University of Pittsburgh, who has been using a laboratory afterglow source of the OI 630 nm emission to determine the interorder separation between the two wavelengths of cerium and hafnium and the central position of the oxygen emission.

Figure 17 summarizes in matrix form the possible choices for the different SOFDI filters. On the basis of the possible wavelengths

we chose to include hafnium and cerium lamps in the calibration source together with a frequency stabilized 632.8 nm HeNe laser. The hafnium source will be particularly valuable for the O^+ ion drift measurements at 732 nm because there are two spectral lines at 7320.0575 Å and 7321.7616 Å that will be especially helpful in determining the Doppler reference calibration.

SOFDI Spectral Lamp Matrix

Desired Spectral Line (Relative Intensity - RI)

		5677	6300	7320	8400
Closest Hollow Cathode Lamp (Fill Gas)	Europium Eu (Ar Ne)	5677.14 (200) 5579.63 (75) 5580.03 (120)	6299.77 (170) 6303.41 (230) Eu II		
	Cerium CE (Xe)		6300.21 (23) 6295.58 (35) 6299.51 (28)		
	Hafnium Hf (Ar Ne)	5575.86 (55)	6299.54 (22w)	7320.05 (75) 7321.76 (16)	
	Ytterbium Yb (Ar Ne)				8400.01 (20)
	Scandium Sc (Ar Ne)				8396.83 (1) 8402.96 (9d) 8405.65 (6)
Close Gas Spectral Lines	Neon Ne	5576.90 (35)	6304.79 (100)		
	Argon Ar	5572.54 (10) 5574.23 5581.87	6296.87 (7)	7316.01 (25)	
	Xenon Xe		6300.5? (250) Xe II		

* w,d = Wide, diffuse, hazy, etc.

Figure 17: Table summarizing the list of possible calibration spectral wavelengths for the selection of SOFDI filters.

The calibration source chamber was mounted within the SOFDI etalon chamber with provision for insertion of the calibration source emission through a fiber optics cable that provided the desired diffusion of the lamp emission. A movable mirror stage provided the means for passing the lamp emission into the optical axis in front of the filter wheel.

However, an important issue in carrying out Doppler shift determinations is the instrumental stability with respect to pressure and thermal fluctuations. The former requires a precise pressurization of the etalon chamber shown in Figure 16 to avoid modulation of the Doppler reference by atmospheric pressure fluctuations that will affect the optical path distance through the etalon plates. In performing the design it became apparent that the enclosure needed to have inflexible thick walls if 1 ms^{-1} stability

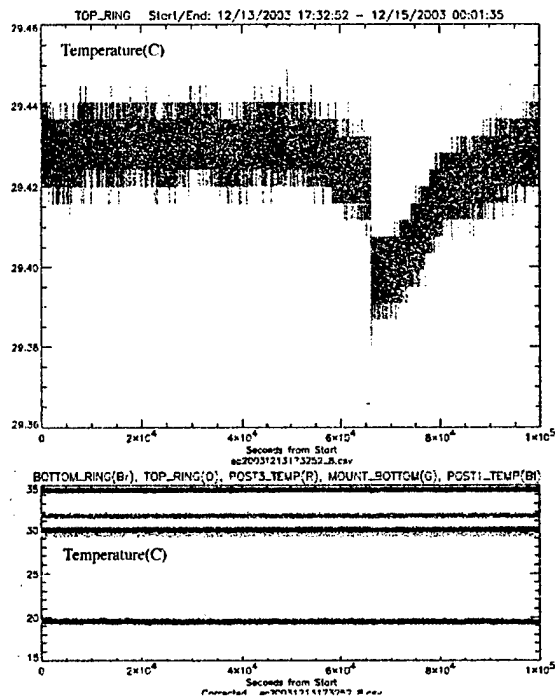were to be achieved. This proved to be helpful in achieving thermal stability as well.

Figure 18: Coarse and fine scale plots of temperature readings of the HRE SOFDI etalon temperature.

The other source of instability is thermal. This requirement means that the etalon chamber be thermally stabilized with respect to room temperature changes to within a small fraction of a degree. A pressure gauge capable of monitoring pressure fluctuations equivalent to 1 ms−1 variations was found and installed in SOFDI. Careful design of the thermal controller circuitry combined with the high thermal inertia represented by the thick walls of the pressure chamber achieved the phenomenal level of thermal stability of 0.015 °C. This is documented in the results shown in Figure 18, which presents plots of the temperature readings obtained over the period of sixteen hours for several different sensors. The glitch seen in this plot is an artifact related to the nature of the data taking of the sensor measurements.

11   SOFDI results

The integration phase of SOFDI went forward reasonably well. The SOFDI optics were assembled in the clean room and then transferred to the SOFDI trailer for installation within the pressure chamber. Several difficulties were encountered as the various pieces were assembled but these problems were resolved without difficulty. The FLI camera initially proved to be somewhat temperamental but this appeared to be a moisture problem that was treated satisfactorily with a rare gas refill of the CCD cavity by FingerLake Instrumentation. The CLIO optic needed to be shimmed a bit to compensate for an error of 1 mm made by the machine shop fabrication of the mount. There was a glitch in which the cycling of the air conditioning would cause the filter wheel to cycle to another position. This was fixed by re-routing the cabling. The collimation of the fiber optics cable signal from the telescope to the fiber optics cable needed to be improved. This was achieved by using the telescope eye piece and adjusting the focal length to obtain the best match of the telescope field of view with the fiber angular field.

The question of calibration of the pointing of the telescope is an issue that will require further work during the commissioning process of SOFDI at any desired location. The SOFDI datataking software has been written to point the telescope with reference to trailer coordinates. What will be necessary is to calibrate these coordinates so that a conversion can be achieved from these trailer coordinates into azimuth and zenith angle coordinates. A CCD camera, a secondary Meade electronic eyepiece (#07166) can be inserted into each telescope system in place of the eyepiece so that the star field can be observed on a TV monitor. By tracking bright stellar objects such as Sirius it will be possible to obtain the necessary calibration pointing coefficients with an accuracy exceeding 2 arc minutes. This precision will be important in regard to the measurement of ver-
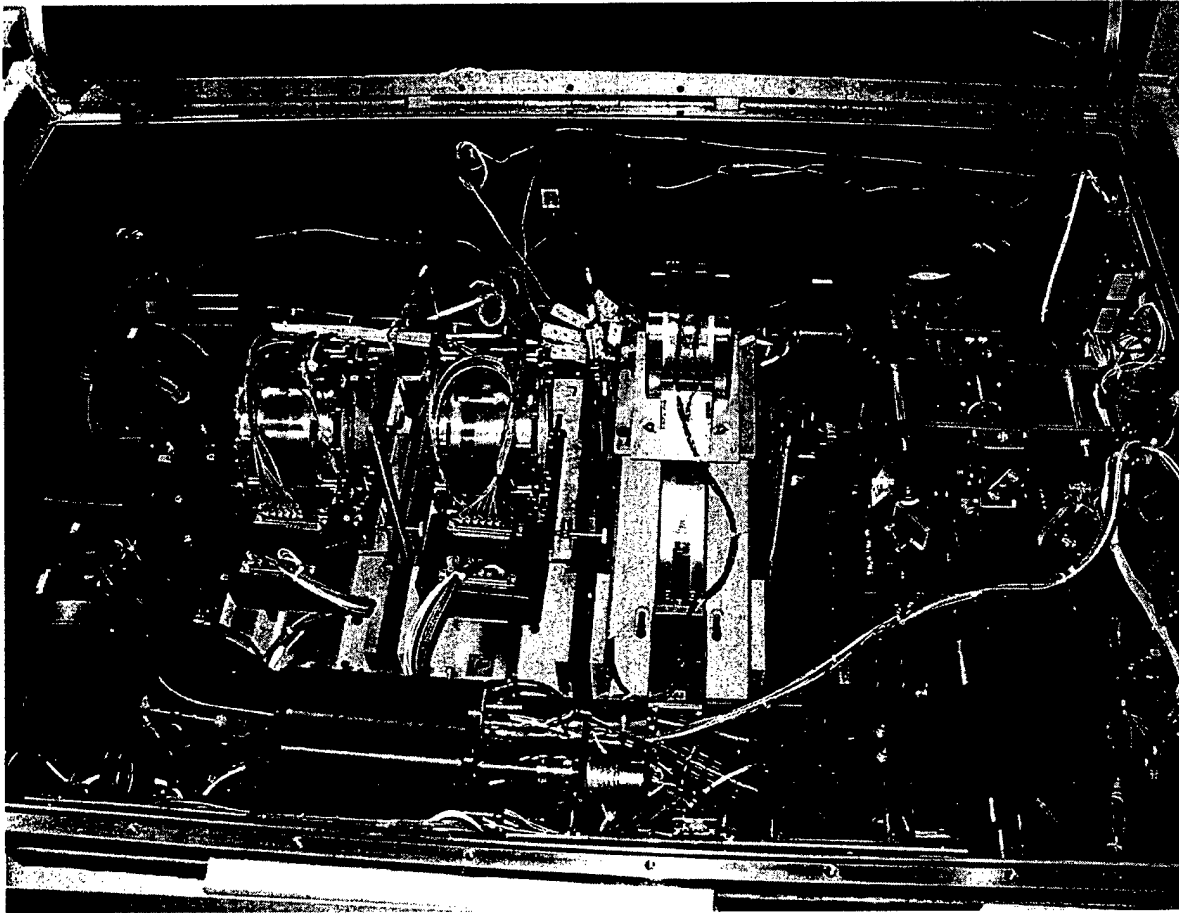
Figure 19: View of SOFDI pressure chamber interior and the three etalons, LRE, MRE, and HRE(inserted in the optical path), arranged from left to right. The two turning mirrors seen in the left and right corners of the chamber fold the optical path into the dimensions of the chamber. The CLIO extender, the CLIO, and the camera are located in the front right corner. The filter wheel is located in the left corner and the calibration source is in the front center area.

tical winds which will require the precise orientation of each telescope toward the zenith.

Figure 19 presents an interior view of the SOFDI pressure chamber showing the optical components of the instrument. The fiber optics are mated to the input chuck at the far left, the three etalons are evident mounted on the movable slides, and the CLIO extender, the CLIO, and the FLI camera may be seen to the right of the figure.

Figure 20 presents one of the first views of the HRE SOFDI ring pattern seen for the HeNe

emission. The etalon posts are optically contacted by TecOptics, and these are expected to be robust against vibration. However, inspection of the interferogram in each of the four quadrants of the plates isolated with a small aperture as illustrated by one plot presented in Figure 22 illustrates that there is a problem with the flatness of the HRE plates. It is observed from this figure that there is broadening and displacement between the five fringes of the full aperture plot and the one-inch aperture plot. We infer from this that one of the optical con-

tacts of the HRE etalon has broken loose resulting in a bending of the plates as mounted with the HRE mount. What this means is that the plates need to be returned to the TecOptics vendor for repair.
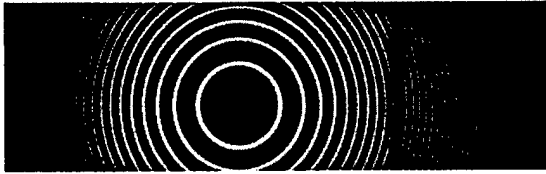

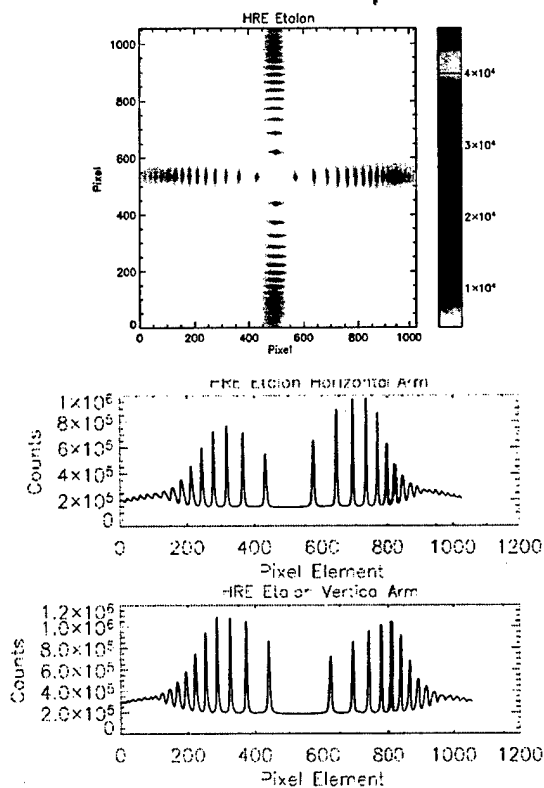Figure 20: High resolution etalon interferogram for the HeNe 632.8 nm emission.

Figure 21: High resolution etalon interferogram for the HeNe 632.8 nm emission. This view illustrates the low finesse of the outer orders for each of the four arms. Investigation found that the CLIO extender optics needed an improved field lens to improve the uniformity of the image.
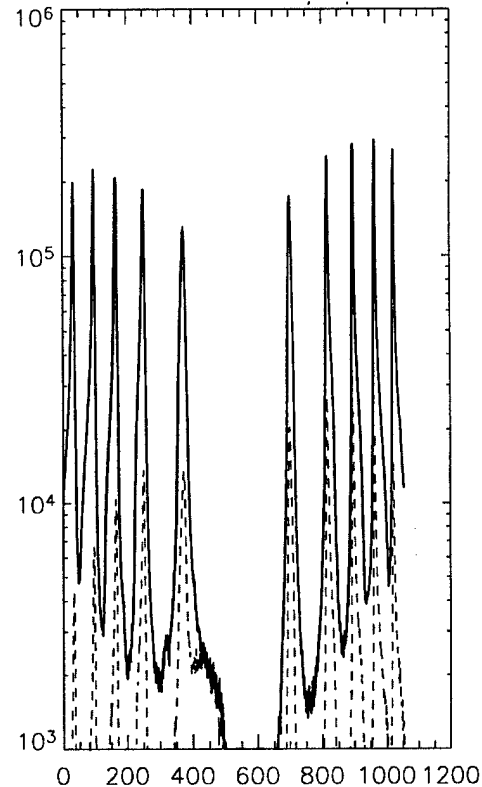

Figure 22: High resolution etalon interferogram for the HeNe 632.8 nm emission observed in one of the four quadrants of the HRE etalon. The black plot is the interferogram for the full aperture and the red is the interferogram observed for the case in which the aperture was mounted in the top central region of the etalon aperture. The displacements between the peak positions of the full-aperture passbands and those of the one-inch aperture passbands combined with the broadening of the full-aperture passbands compared with the one-inch aperture passbands indicate that the HRE etalon is not as flat as indicated by the specifications.

In Figure 21 the CLIO transformation of the HRE rings and the twelve orders for each arm of the QuadCLIO array may be discerned in this view. The light for each of the 12 orders

19

of the HeNe interferogram is concentrated into about 1% of the 10^6 pixels. The linear spread (vertical or horizontal) in each of the 12 CLIO orders for each arm is caused by the optical dispersion of the objective lens. What would be applied in the data analysis process is the integration of the signal across the columns (or rows) for each CLIO order to finish the 2D integration of the signal into a 1D interferogram that can be analyzed to extract the Doppler position, the Doppler broadening, and the airglow intensity and background continuum.

The CLIO HeNe results for the triple etalon configuration as obtained in the most recent spectrum are presented in Figure 23. One sees from this figure that the flatness of the HRE etalon is affecting the appearance of the side bands for the bottom arm of the interferogram. The adjacent sideband of the triple etalon instrument function for the bottom arm is much too bright. The theoretical simulation shows that the ratio of the main peak to the most intense sideband should be ~15 and what is seen here (from cross cuts) is about a ratio of 9 to 1.

It turned out that the image reaching the CLIO extender section was not in the sharp focus required for the QuadCLIO extender optics to work properly. The result was that the sidebands of the CLIO image were too strong. Dr. Paul Hays applied the optical model to study more precisely the SOFDI optics and found a simple modification that improved the quality of the image by adding a corrective field lens. The spherical aberration problem was generated by off-axis rays that had not been considered in the original optical ray-tracing design. However, unfortunately, this modification resulted in an another problem in that the number of orders decreased from 12 to 5. This can be treated by adjusting the position of the objective lens to decrease the magnification of the image before entrance into the collimator section located ahead of the elalon optics. Why this problem occurred is not yet understood and will continue to be the subject of investigation.
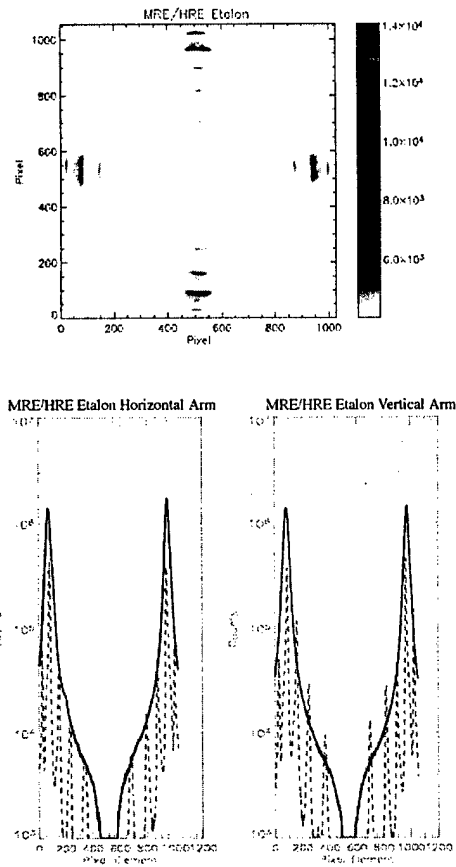

Figure 23: The HRE+MRE CLIO image of the HeNe source after installation of the CLIO-corrected optics. The top half of the figure represents the 2 D view and the bottom half the interferograms for the horizontal and vertical cross cuts of the 2D view. The black curve is the combined interferogram for the MRE + HRE alignment. The red curve is the plot of the HRE interferogram for the HRE alone.

We are still in the early phase of learning how to make the appropriate adjustments to achieve the optimal alignment. This is a very important step in the application of the SOFDI instrument to the measurements of daytime winds. As was demonstrated in the simulation presented above, the OI 630 nm dayglow lies within a Fraunhofer valley that is of the order of 5 percent. If the sidebands are significant in intensity, then it will be difficult to extract the

630 nm dayglow profile out of the valley structure through application of the forward model for the SOFDI instrument function.

The plan for the future at present is to reinstall the HRE etalon once it has been repaired and to check out the optics in regard to how well the observed performance matches the expectation based upon a model for the combined triple etalon transmission function. Then we will carry out trial operations of the trailer in upstate New York in collaboration with the Millstone Hill Observatory suite of radar and optical instrumentation. We expect to ship SOFDI to Peru in the late fall of 2004 for installation at the chosen observatory site near the magnetic equator.

Figure 24 illustrates the HRE spectrum seen with the source emission from the cerium lamp. The structure is considerably broader than what is seen in Figure 21.
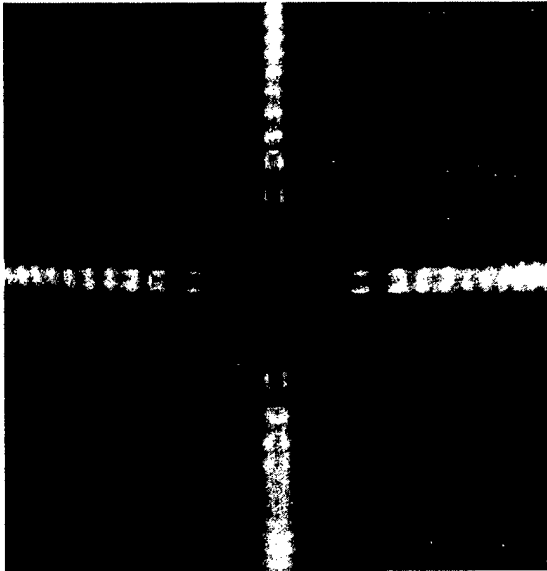

Figure 24: HRE spectrum from the cerium source.

12 Summary-SOFDI new technical innovations

Here we list the several new ideas that went into the design and construction of SOFDI.

• Perhaps the most interesting technical innovation is the use of the QuadCLIO optic as a means for collecting light simultaneously from four telescope systems pointing in four separate directions. This comes with the penalty of losing half of the light due to the transmission loss of the fiber optics cables. However, the approach of sequential scanning would have lost a fraction of the total signal due to the time required to move from one direction to another. The CLIO provides the advantage of improving the ratio of signal to noise for weak airglow signals, which is why it was employed. It would not be required for the auroral region where there is much more signal available for the measurements.

• The QuadCLIO extender is also an important innovation because it meant that a low cost CCD camera could be employed for the detector, the process of integration and assembly of the optics is more straight-forward, and it solves the problem of overlapping fields of view that would otherwise take place.

• The ability to switch from the nighttime mode featuring the HRE etalon to the multiple etalon configuration is also a unique innovation never before tried in Fabry-Perot interferometry. Our measurements indicate that this can be achieved remotely within several minutes without loss of alignment. This makes it possible to utilize an expensive instrument through the day and night continuously with a change taking place at twilight to switch from the daytime setup to the nighttime setup or the reverse.

• The use of fiber optics cables is an innovative way of passing the light from the telescope to the FPI instrument. It allows the pressure chamber to be mounted within the trailer at a location that is convenient for troubleshoot-

ing and where the optimum thermal control can be achieved. Such a location also allows the mount for this chamber to be isolated from the trailer by stiff springs to eliminate the effects of low frequency vibrations.

- The SOFDI observatory is an example of an instrument designed to be fielded at a remote site but controlled over the Internet in all phases of its operation. As an example, this ability for remote access via Internet meant that programming and testing could be achieved with considerable ease without requiring the operator be at the SOFDI computer.

- The attention paid to the SOFDI Doppler calibration at 630 nm with the Hf and Ce sources is unique. SOFDI will have the ability to measure for the first time Doppler shifts with reference by means of a secondary standard to a laboratory reference position representing the zero line-of-sight Doppler shift. This feature combined with the extraordinary stability of SOFDI means that vertical winds of several ms^{-1} can be measured without making an assumption as to the long-term average of the vertical wind, which is normally taken to be zero. The accuracy of horizontal wind measurements will be improved by removing the uncertainty introduced by the lack of an absolute Doppler reference.

An important issue is the question of system transmission through the three etalons and the other optical components. Figure 25 illustrates schematically the transmissions of the individual section of the SOFDI instrument that were measured. The overall transmission of the system including the filter transmission is ~3%. This is a reasonable result considering the large number of optical components that exist in the SOFDI instrument.

13   Instrumental   problems still remaining

- The question of stability is an important concern that enters into the consideration of SOFDI applications in regard to how frequent calibration might be required. We have carried out several long runs and identified pressure leaks as being the most significant source of instrumental drifts. Once the optics problems have been settled, we are optimistic that this situation will improve. At present the stability is seen to be about 10 ms^{-1} per hour which is not nearly as good as what we had hoped for. We expect this result would improve once the we can avoid the need to open and reseal the pressure chamber in testing the alignment of the optics.

- The sideband rejection of the triple interferogram illustrated by Figure 23 is disappointing. We expected from the realistic modeling studies carried out that the ratio of the main transmission peak to the first sideband would be $\sim$ 20 to one but instead, we find for the optimal setup a ratio of about 9 to one, with one bad arm. The small aperture interferograms illustrate that the HRE etalon is not flat as the several interferograms do not line up as they should in the plot shown. This is a problem most likely a result of the HRE plates not being as flat as expected by the specifications. We believe that this can be repaired by the vendor who will remove the plates and redo the optical contacting of the posts. This will cause a three to five weeks delay most likely for the turnaround of the plates. However, the problem is simple to fix.

- Probably the biggest surprise encountered in the whole project came when the CLIO extender was re-engineered to include a field lens that was needed to improve the optical quality of the image. It appears that the CLIO extender optics was fabricated by the vendor Luminflow with optics that did not meet the specifications

laid out by their ZEMAX design. The removal of this problem to take advantage of the fast optics of the SOFDI instrument will require a relocation of the objective lens ahead of the collimator section so that the image is de-magnified. This will be attended to once the HRE etalon has been reinstalled. There is no impact upon SOFDI ability to observe the dayglow as only one of the HRE orders is utilized. The error bar in the nighttime measurements would be increased by some 40 % as a result. However, it is expected that the proposed fix would restore the set of 12 fringes that had been originally observed.
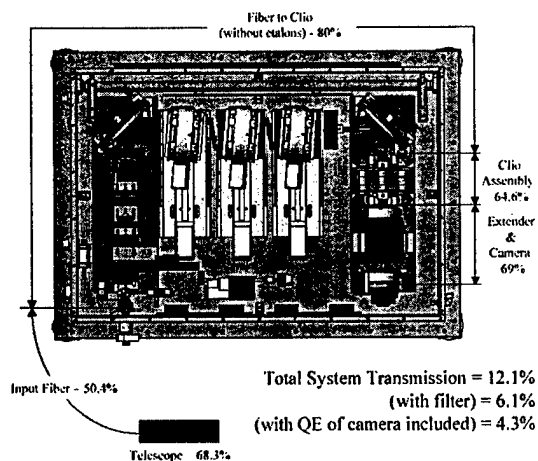

Figure 25: SOFDI optical layout illustrating measured transmission through each section marked.

14 Appendix A - SOFDI telescope pointing algorithm

The light that is introduced into the SOFDI instrument is gathered by four independent telescopes mounted in separate domes, each system housing a steerable mirror that directs light into a telescope and ultimately into a fiber optic cable that is fed into SOFDI. As depicted in Figure 26, within each dome is mounted the two pieces of a disassembled four inch Meade ETX telescope. Above each telescope objective lens is a fixed 45° mirror. The telescope base mount that normally holds and steers the Meade telescope was mounted horizontally at a fixed location across from the 45° turning mirror. Another tuning mirror was set into the base mount brackets so as to direct incoming light from a particular zenith angle and azimuthal angle in the sky over to the 45° degree turning mirror where it is reflected into the telescope objective lens. The base mount is steerable via a computer connection to the Meade interface. Also within each dome is a heater/fan unit to minimize condensation and increase airflow. Also mounted within each dome are two white diffuser plates located perpendicularly from the mount/turning mirror optical path. These diffusers will allow the telescopes to observe the scattered light of the solar spectrum without having to actually look at the sun, which could seriously harm the SOFDI optics.

Due to the concern regarding the possible obstruction of the line-of-sight between a source region in the sky and any one telescope by the all-sky imager dome, as well as the space constraints within the domes themselves, each telescope was limited in elevation and azimuthal range by limit-switches, which restricts each telescope field of view(fov) to a range of angles. The word "telescope" is used here with the understanding that it is really the turning mirror, controlled by the telescope base mount drive, that directs light into the fixed objec-
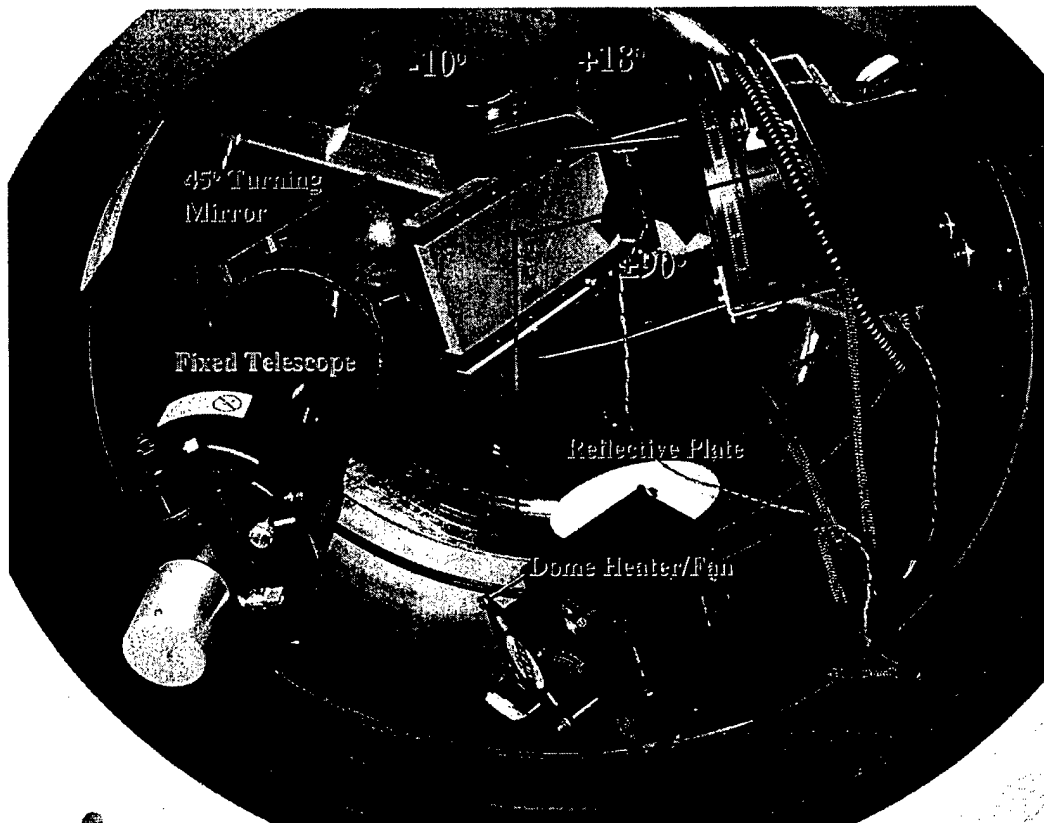
Figure 26: One of the four telescope systems mounted within a dome The mirror above the vertical telescope section (objective lens) is fixed while the other mirror may rotate about either of the two axis shown. The range of tilt angles is + 18 to -10° about the mirror axis, and the scanner mirror assembly can be rotated ±90° about the orthogonal horizontal axis. The object in the lower portion of the image is a dome heater intended to prevent dome condensation.

tive lens of the telescope. As depicted in Figure 26 and tabulated in Figure 27, each telescope mount has two separate angular ranges: a rotation of ±90° about one horizontal axis, and -10°/+18° about the orthogonal horizontal axis. The combination of the four telescope systems makes possible the almost complete coverage of the sky, as is tabulated in Figure 27 and depicted in the telescope fov schematic shown in Figure 28.

In standard operation, the user will use an IDL procedure that displays a console very similar to Figure 28. For each telescope, the user will select the desired geophysical zenith and azimuth angles for that telescope system. The procedure will then compute and return the positions to which each of the two coordinates of the telescope steering mirror is to be set so that the selected geophysical coordinates are reached. The procedure that does this transformation is outlined as:

1. Az and Zen angles for a particular telescope are chosen.

2. For each telescope, these values are compared to the allowable angular ranges for both zenith and azimuth axis so that the quad-

	Mount Elevation	Mount Azimuth	Geophysical Zenith Range	Geophysical Azimuth Range[*]
Telescope 1	-10° / +18°	±90°	-20° / +36°	150° - 330°
Telescope 2	-10° / +18°	±90°	-20° / +36°	240° - 60°
Telescope 3	-10° / +18°	±90°	-20° / +36°	300° - 120°
Telescope 4	-10° / +18°	±90°	-20° / +36°	0° – 180°

[*]With Research Trailer pointing due North and telescope mirror elevation at 0°.

Figure 27: Table presenting the range of elevation and azimuth angles for each of the four telescope systems relative to the trailer orientation in the north-south direction.

rant, relative to the particular telescope, is determined.

3. These values are used in the appropriate set of equations to determine the telescope steerable mirror coordinates relative to the home position.

To ensure that the telescope does indeed move to the desired location, the absolute "home" position will be calibrated by reference to stellar sources observed with a CCD camera inserted in place of the telescope eyepiece. All user-specified positions are then based on this calibrated home position. The accuracy of the home positions would be verified with monthly calibrations to eliminate the possibility that the telescope mount stepper motors may lose their accuracy/repeatability due to possible slippage in the telescope drive gearing.
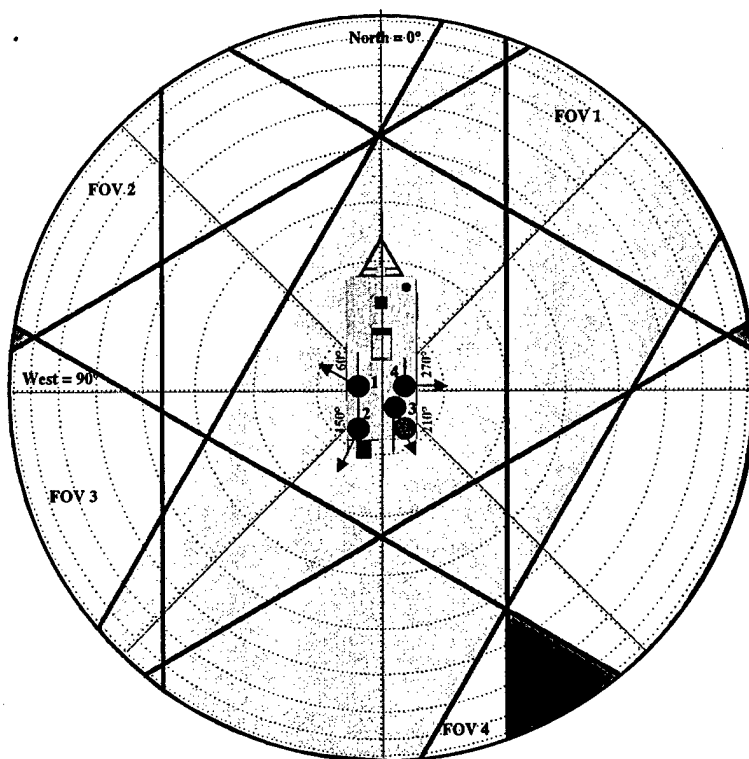
Figure 28: A cartoon illustrating the field of view coverage for each of the four telescopes relative to the longitudinal axis of the trailer.